J. Fluid Mech. (1971), *vol.* 50, *part* 1, *pp.* 1–16
Printed in Great Britain

Unsteady multicellular viscous vortices

By P. G. BELLAMY-KNIGHTS
Department of the Mechanics of Fluids, University of Manchester

(Received 27 April 1971)

The problem of a viscous vortex core embedded in an unsteady outer potential swirling flow is considered. By introducing a suitable similarity variable, the full Navier–Stokes equations for the unsteady axisymmetric flow of an incompressible fluid are reduced to two ordinary differential equations. These are solved numerically. When the radial flux of a particular outer potential flow satisfies certain conditions a family of three-cell core structures is possible. This family is not represented by any known analytical solution.

This work is useful for studying meteorological flow systems such as tornadoes. In particular, it suggests how two- and three-cell structures can develop from a one-cell structure and also shows the sensitivity of the core flow to small changes in the outer potential flow.

1. Introduction

In an earlier paper (Bellamy-Knights (1970), to be referred to hereafter as I) a theoretical study of a special case of the unsteady axisymmetric swirling flow of a viscous incompressible fluid was made, in which analytic solutions were possible. One object of that work was to analyze the effect of radial outflow or inflow on the decay of circumferential velocity in the core of a viscous vortex. For the special case considered the flow was bounded by a plane, $z = 0$, perpendicular to the axis of symmetry and, with increasing radius, tended asymptotically to a potential flow solution for which the circulation was constant. It was also assumed that the radial and tangential velocity components were independent of axial distance z.

Such a model has been found useful for considering meteorological phenomena such as tornadoes (Morton 1966). The general physical validity and limitations of such a model were discussed in I. For example, these solutions allow neither lateral spreading of the vortex core with increasing height nor a free stagnation point. Also, boundary-layer effects over the plane boundary are neglected and certain boundary conditions are rarely, if ever, approximated in reality. These solutions are, however, useful for considering the core flow in an axial region for which the boundary-layer effects of the ground, $z = 0$, and the lateral core expansion can be neglected.

One- and two-cell analytical solutions of this category, which satisfied the full Navier–Stokes equations, were obtained and described in I. (The boundary of a cell is defined as a cylinder on which the radial velocity is zero.) Outside the vortex core both the one- and two-cell solutions had the same asymptotic

behaviour as the potential flow solution for which the axial velocity is independent of radius and the circulation is constant. This suggested that there might be other solutions with different core structures, asymptoting to the same potential flow solution as these two analytical solutions. No other analytical solutions were discovered so the investigation was extended numerically. The results are reported in this paper.

Cylindrical polar co-ordinates r, θ, z are used and u, v and w refer to the radial, tangential, and axial velocity components respectively. Time, density, pressure and kinematic viscosity are denoted by t, ρ, p and ν respectively.

In I a particular class of exact solutions of the Navier–Stokes equations was considered. These flows were characterized by velocity components of the type

$$u = u(r,t), \quad v = v(r,t), \quad w = zW(r,t). \tag{1.1}$$

Then the axial momentum equation could be written in the form

$$\frac{1}{\rho}\frac{\partial p}{\partial z} = z\left\{-\frac{\nu}{r}\frac{\partial}{\partial r}\left[r\frac{\partial}{\partial r}\left(\frac{1}{r}\frac{\partial g}{\partial r}\right)\right]+\frac{1}{r}\frac{\partial^2 g}{\partial r\,\partial t}+\frac{g}{r}\frac{\partial}{\partial r}\left(\frac{1}{r}\frac{\partial g}{\partial r}\right)-\left(\frac{1}{r}\frac{\partial g}{\partial r}\right)^2\right\}, \tag{1.2}$$

where

$$g(r,t) = ru. \tag{1.3}$$

Under certain restrictions on the form of $\partial p/\partial z$ (see (1.13) below), similarity solutions of (1.2) can be obtained in terms of the similarity variable

$$\eta = r^2/4\nu t. \tag{1.4}$$

First, it is convenient to non-dimensionalize the dependent variable g by putting

$$g = -2\nu f(\eta), \tag{1.5}$$

where the minus sign is introduced so that there is radial inflow when f is positive. Then (1.2) reduces to

$$[\eta f''+\eta f']'+ff''-f'^2 = (t^2/\rho z)\,\partial p/\partial z, \tag{1.6}$$

where primes denote differentiation with respect to η.

The radial velocity component is zero on the axis of symmetry so

$$f(0) = 0. \tag{1.7}$$

The solution is required to asymptote to an irrotational swirling flow at infinity where the velocity components are

$$u = -\gamma r/2t, \quad v = K_c/r, \quad w = \gamma z/t. \tag{1.8), (1.9), (1.10}$$

The parameter γ characterizes the scale of the asymptotic velocity field and $2\pi K_c$ is the circulation. Thus as $\eta \to \infty$,

$$f \to \gamma\eta + B, \tag{1.11}$$

where B is an arbitrary constant.

For flows of type (1.1), differentiating the radial momentum equation with respect to z gives

$$\partial^2 p/\partial r\,\partial z = 0. \tag{1.12}$$

Hence the axial pressure gradient is independent of radius and is therefore determined by its value in the outer potential flow. This is reminiscent of boundary-layer theory for which the pressure is constant through the thickness of the boundary layer and therefore determined by the mainstream conditions. In the present rotating flow problem the axial pressure gradient (for a fixed value of z and t) is constant through the vortex core and is therefore determined by the outer potential flow. In the outer potential flow the axial pressure gradient is obtained by substituting (1.8) to (1.10) into the axial momentum equation. This gives

$$(t^2/\rho z)\,\partial p/\partial z = -\gamma(\gamma-1). \tag{1.13}$$

Hence (1.6) becomes

$$[\eta f''+\eta f']'+ff''-f'^2+\gamma(\gamma-1) = 0. \tag{1.14}$$

In I, for flows of the type defined by (1.1), the circumferential momentum equation reduced to

$$\frac{\partial K}{\partial t}+\frac{g}{r}\frac{\partial K}{\partial r} = \nu r\frac{\partial}{\partial r}\left(\frac{1}{r}\frac{\partial K}{\partial r}\right), \tag{1.15}$$

where

$$K = rv. \tag{1.16}$$

It is now assumed that K is a function of η only. Then, non-dimensionalizing K,

$$K = K_c h(\eta). \tag{1.17}$$

Equation (1.15) then reduces to

$$\eta h''+\eta h'+fh' = 0. \tag{1.18}$$

The circumferential velocity component is zero on the axis of symmetry so

$$h(0) = 0. \tag{1.19}$$

Also, from the outer potential solution, as $\eta \to \infty$,

$$h \to 1. \tag{1.20}$$

The integration of (1.14) and (1.18) is complicated by the nature of the boundary conditions, which include conditions at both ends of the range. Equation (1.18), for h, is linear and poses no problem once f has been determined from (1.14). This, however, is nonlinear. The approach used is to replace the outer boundary condition on f by a tentative value, A say, of f' on the axis, i.e.

$$f'(0) = A, \tag{1.21}$$

and proceed outwards from the axis to determine the numerical solution. Equation (1.14) shows that as $\eta \to 0$,

$$f''' \to -f''-\{f''+f'+ff''-f'^2+\gamma(\gamma-1)\}/\eta. \tag{1.22}$$

It follows that if f''' is to be finite on the axis, as seems physically reasonable, then

$$f''(0) = (A-\gamma)(A+\gamma-1). \tag{1.23}$$

The three conditions on f, f' and f'' on the axis given by (1.7), (1.21) and (1.23)

enable (1.14) to be solved by marching techniques. This was done for various values of A. As might be expected, solutions compatible with the outer boundary condition are not obtained for all values of A.

For two special values of A analytical solutions can be obtained. First, it is apparent that when $A = \gamma, f''(0)$ is zero and the solution of (1.14) is

$$f = \gamma\eta. \tag{1.24}$$

Then the solution for h obtained from (1.18) is

$$h = 1 - \exp\{-(1+\gamma)\eta\}. \tag{1.25}$$

The other analytic solution is obtained when $A = -2\gamma$. In this case the solution of (1.14) is

$$f = \gamma\eta - [3\gamma/(1+\gamma)][1 - \exp\{-(1+\gamma)\eta\}]. \tag{1.26}$$

Then (1.18) gives the corresponding solution for h in closed form.

Provided that $1+\gamma > 0$ both these solutions will satisfy the outer boundary conditions (1.11) and (1.20). The first solution corresponds to the one-cell solution of Rott (1958) and the second solution is an analytical two-cell solution. Both these solutions were considered in detail in I. This paper extends the results of I by showing that there are values of A other than $A = \gamma$ and $A = -2\gamma$ which give solutions of (1.14) and (1.18) satisfying the boundary conditions (1.7), (1.11), (1.19) and (1.20). It will be shown that an infinite number of such solutions is possible for each value of γ in the range $-1 < \gamma < \frac{1}{2}$. These solutions are obtained when A lies in the range $2\gamma - 2 < A < 1 - \gamma$.

Two particular values of A in this range give the analytical solutions referred to above. As A varies over the permitted range of values solutions with various core structures are obtained, each tending asymptotically to the same outer potential flow solution specified by γ. Apart from one- and two-cell structures similar to the analytical solutions obtained previously, three-cell structures were discovered for a subrange of A. These three-cell solutions occurred only when γ was negative, that is, when the outer potential flow was radially outwards.

2. Numerical integration of equations

Restricting attention to flows of the type described by (1.1) and assuming that the solutions depend only on a similarity variable η, proportional to r^2/t, the complete Navier–Stokes equations have been reduced to two ordinary differential equations

$$[\eta f'' + \eta f']' + ff'' - f'^2 + \gamma(\gamma - 1) = 0 \tag{2.1}$$

and

$$\eta h'' + \eta h' + fh' = 0, \tag{2.2}$$

subject to the boundary conditions

$$f(0) = 0, \quad h(0) = 0 \tag{2.3), (2.4}$$

and, as $\eta \to \infty$,

$$f \to \gamma\eta + B, \quad h \to 1. \tag{2.5), (2.6}$$

The physical problem of solving (2.1), subject to a boundary condition at

infinity as well as at the axis, is made more amenable to numerical treatment by replacing the outer boundary condition by an additional condition on the axis, as described in § 1. The numerical problem is therefore to solve (2.1) subject to the initial conditions

$$f(0) = 0, \quad f'(0) = A, \quad f''(0) = (A-\gamma)(A+\gamma-1). \quad (2.7), (2.8), (2.9)$$

After obtaining the solution for f it is in principle possible to write the solution to (2.2) in closed form, i.e.

$$h = M\int_0^\eta \exp\left[-s-\int_0^s \frac{f(q)}{q}\,dq\right] ds, \tag{2.10}$$

where

$$\frac{1}{M} = \int_0^\infty \exp\left[-s-\int_0^s \frac{f(q)}{q}\,dq\right] ds. \tag{2.11}$$

In practice, however, it is simpler to replace boundary condition (2.6) by the condition

$$h'(0) = 1, \tag{2.12}$$

and to solve (2.2) by marching techniques simultaneously with (2.1). This results in some value for $h'(\infty)$, say N. Since (2.2) is linear in h, the required solution for h satisfying the boundary condition (2.6) can be obtained by dividing the computed solution by N, provided that N is finite.

Equations (2.1) and (2.2), subject to boundary conditions (2.7), (2.8), (2.9), (2.4) and (2.12), were solved simultaneously on an I.C.T. Atlas computer using the Kutta–Merson fourth-order integration method. This is a modification of the standard Runge–Kutta procedure which automatically adjusts the step length to obtain a prescribed accuracy.

The solution is governed by the parameters A and γ. If the computed value of f' does not tend to γ as $\eta \to \infty$ or if N is infinite, then the outer boundary conditions are not satisfied, so there is no physical solution for these pre-assigned values of A and γ. For example when $\gamma < -1$ it is found that $f' \to \gamma$ only when $A = \gamma$. In this case, however, N is infinite; alternatively, $A = \gamma$ corresponds to the analytical one-cell solution for which it can be seen from (1.25) that h is unbounded when $\gamma < -1$.

On the other hand, it is found that the outer boundary conditions are satisfied (*a*) for two values of A when $\gamma > \frac{1}{2}$, (*b*) for a limited range of values of A, $2\gamma-2 < A < 1-\gamma$, when $-1 < \gamma < \frac{1}{2}$. (The condition $\gamma < \frac{1}{2}$ is given analytical consideration in an appendix.) The parameter γ defines the scale and sense of the outer potential flow (positive and negative γ referring to radial inflow and outflow respectively). For fixed γ different values of A correspond to different flows in the core region each of which tends to the same potential flow at infinity.

3. Results of numerical integration

A large number of numerical solutions were obtained over the range of real values of γ and A. It was found that the solutions satisfying the outer boundary conditions could be divided into three main categories based on the value of γ, see figure 1.

First, when $\gamma > \frac{1}{2}$ only two values of A, $A = \gamma$ and $A = -2\gamma$, gave solutions. These were of course the analytical solutions already discussed. When other values of A were assigned the computed values of f did not satisfy the outer boundary condition (1.11). For the particular value $\gamma = 0{\cdot}8$, figures 2 and 3

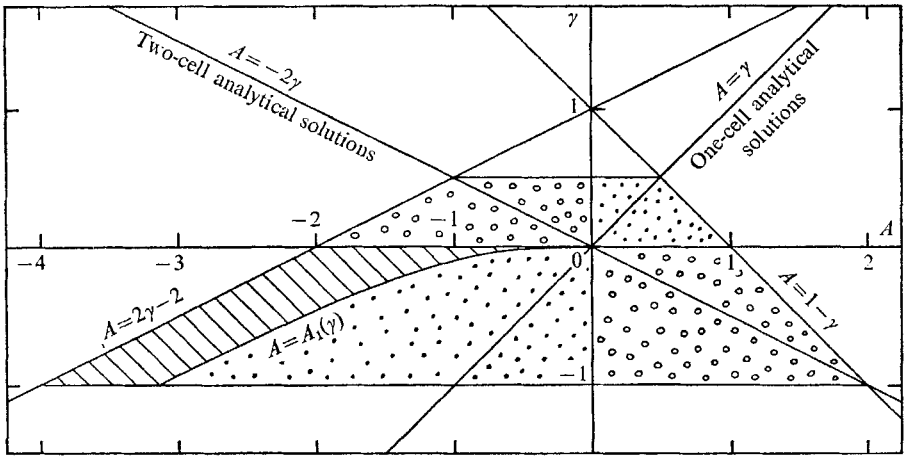

FIGURE 1. Solutions obtained from the parameters γ and A: ▦, one-cell solutions; ⁘, two-cell solutions; ▥, three-cell solutions.

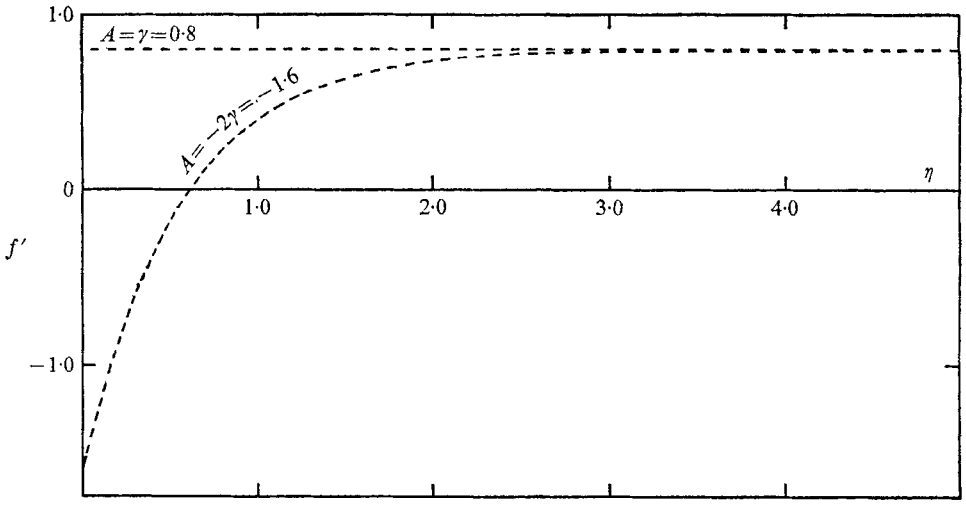

FIGURE 2. f' is plotted as a function of η for two values of A when $\gamma = 0{\cdot}8$.

show f' and f respectively when $A = 0{\cdot}8$ and $A = -1{\cdot}6$. (In figures 2 to 7 the analytical solutions are shown by broken lines.)

Second, when $0 < \gamma < \frac{1}{2}$ solutions were obtained for all values of A within the range $2\gamma - 2 < A < 1 - \gamma$. The number of cells in any particular solution was obtained by inspecting the behaviour of f. Since

$$f = -ru/2v,$$

the radial velocity is zero when $f = 0$. Thus, if f cuts the η axis m times the solution has $m+1$ cells. Similarly, the nature of the axial flow was obtained by inspecting the graph of f'. Since

$$f' = tw/z,$$

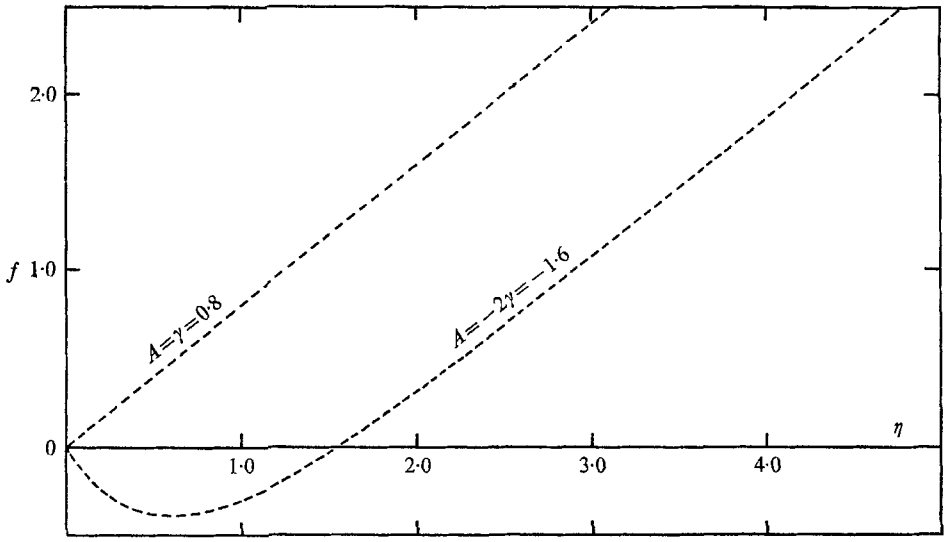

FIGURE 3. f is plotted as a function of η for two values of A when $\gamma = 0{\cdot}8$.

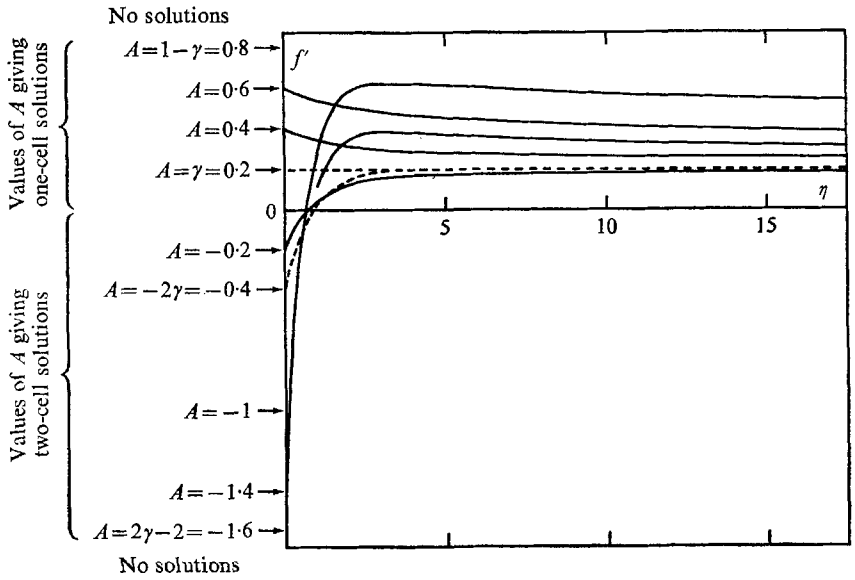

FIGURE 4. f' is plotted as a function of η for various values of A when $\gamma = 0{\cdot}2$.

the axial velocity changes direction when f' cuts the η axis. Thus for the second category it was found that one-cell solutions were obtained when $0 \leqslant A < 1-\gamma$. These solutions were qualitatively similar to the analytical one-cell solution given by $A = \gamma$, which itself belongs to this subrange. When $2\gamma - 2 < A < 0$ two-cell

solutions were obtained which were qualitatively similar to the analytical two-cell solution obtained when $A = -2\gamma$. For the particular value $\gamma = 0{\cdot}2$, figures 4 and 5 show f' and f respectively for typical values of A in the range

$$-1{\cdot}6 < A < 0{\cdot}8.$$

In the above two categories the radial velocity in the outer potential flow was inwards. The most interesting results, however, were obtained in the third and last category, where $-1 < \gamma < 0$, for which the radial velocity in the outer flow was outwards. As for flows in the second category, solutions were obtained

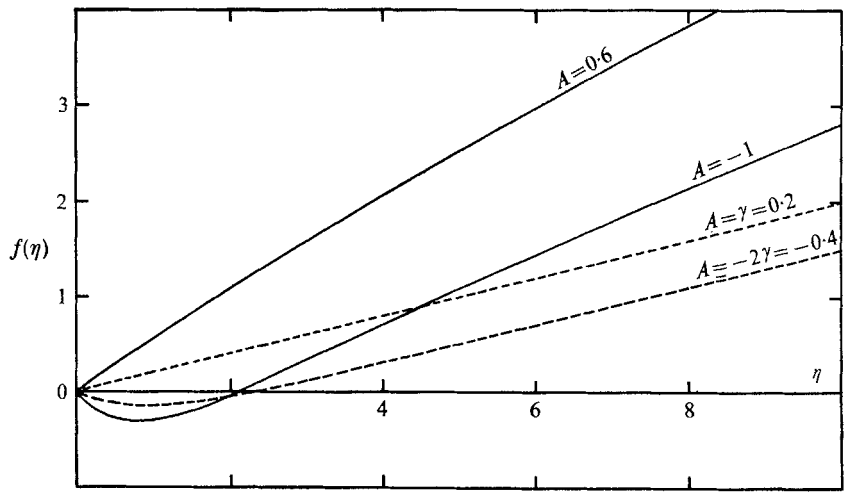

FIGURE 5. f is plotted as a function of η for various values of A when $\gamma = 0{\cdot}2$.

for all values of A in the range $2\gamma - 2 < A < 1 - \gamma$. It is now convenient to divide this range into three subranges as follows. (i) When $0 < A < 1 - \gamma$, two-cell solutions were obtained. (ii) When $A_1 < A \leqslant 0$, one-cell solutions were obtained; A_1 is that value of A for which f touches the η axis. Over this subrange of A, f does not intersect the η axis and the radial velocity is everywhere outwards. For values of A near A_1, however, f' intersects the η axis twice giving solutions with an annular region of reversed axial velocity. (See figure 13, curve (*b*).) This interesting feature suggests how the three-cell solutions (described below) could develop from the one-cell solutions. This development will be described in § 4. (iii) When $2\gamma - 2 < A < A_1$, three-cell solutions were obtained because f cuts the η axis at two points.

For a typical value of γ in the third category, namely $\gamma = -0{\cdot}6$, the computed values of f' and f are given, in figures 6 and 7 respectively, for typical values of A in the subranges described above.

To sum up, the solutions obtained when $-1 < \gamma < \frac{1}{2}$ can be distinguished by the sign of A/γ. If A/γ is negative two-cell solutions are obtained and if A/γ is positive one-cell solutions are obtained except when γ is negative and $A < A_1(\gamma)$ in which case three-cell solutions are obtained, see figure 1.

For each of the solutions for f in the three categories described above the corresponding computed value of h tended monotonically to a finite upper bound

N. Thus, after normalization with respect to N, the outer boundary condition (1.20) was satisfied. Figure 8 shows the computed values of h, before and after normalization, for typical values of γ and A.

The reliability of the computer results was confirmed by comparing the computer results obtained when $A = \gamma$ and $A = -2\gamma$ with the corresponding

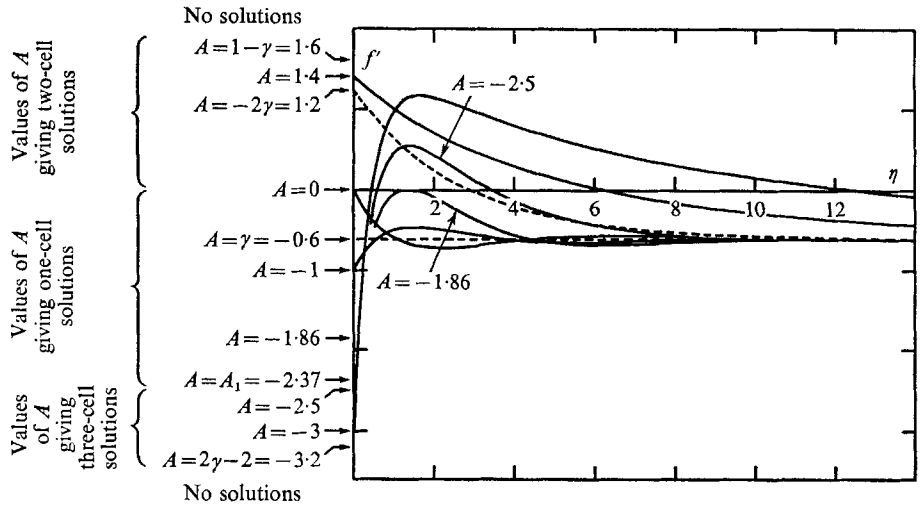

FIGURE 6. f' is plotted as a function of η for various values of A when $\gamma = -0{\cdot}6$.

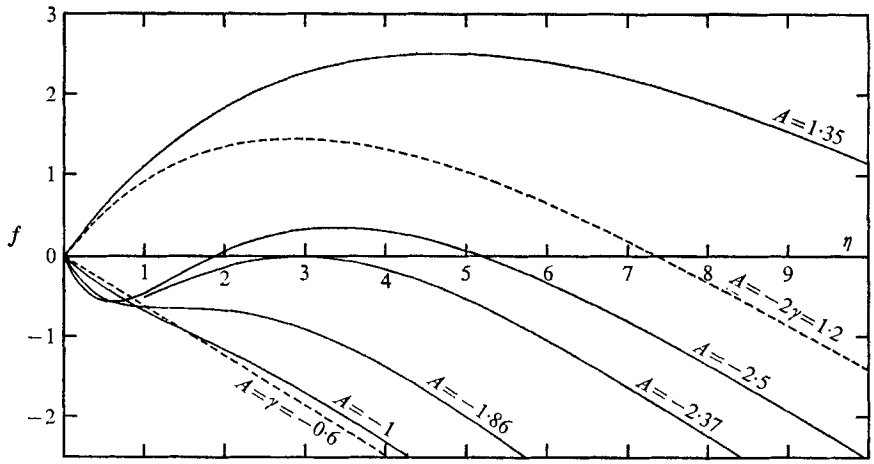

FIGURE 7. f is plotted as a function of η for various values of A when $\gamma = -0{\cdot}6$.

analytical solutions. Although figures 2–8 show results only as far as about $\eta = 20$, some programmes were run as far as $\eta = 2000$. The total error (i.e. discretization error and stability error) was negligible throughout this large range.

When f and h have been computed the velocity components can be obtained from the equations

$$u = -2\nu f/r, \quad v = K_c h/r, \quad w = zf'/t. \qquad (3.1), (3.2), (3.3)$$

Also the stream function ψ is given by

$$\psi = 2\nu z f, \tag{3.4}$$

where the surfaces ψ = constant are stream tubes and the streamlines are spirals lying on these stream tubes. A meridian plane cuts a stream tube in a section which will henceforth be termed a 'streamline'.

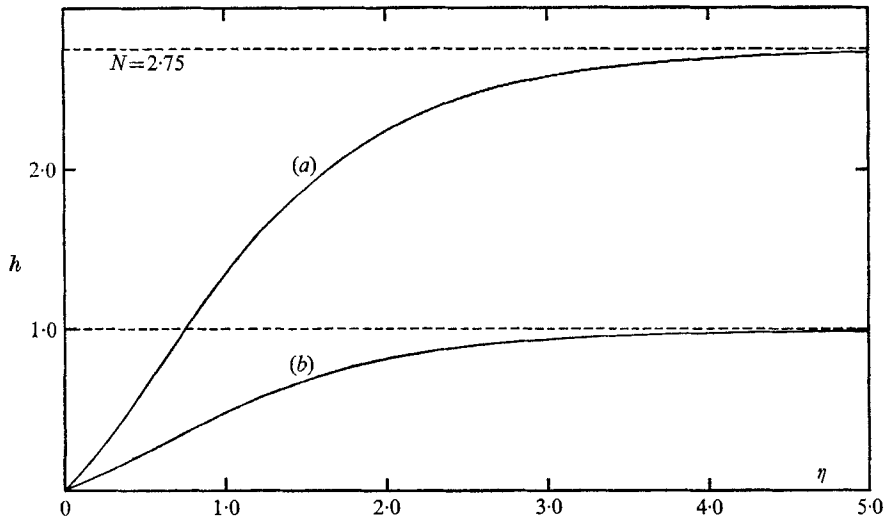

FIGURE 8. h is plotted as a function of η when $\gamma = -0{\cdot}6$ and $A = -2{\cdot}5$ (a) before and (b) after normalization with respect to N.

It will be convenient to introduce an arbitrary length scale, r_0 say, in order to express the variables non-dimensionally. Then non-dimensional quantities, denoted by superscript bars, are defined by

$$(\bar{r}, \bar{z}) = (1/r_0)(r, z), \tag{3.5), (3.6}$$

$$\bar{t} = 4\nu t/r_0^2, \tag{3.7}$$

$$(\bar{u}, \bar{w}) = (r_0/2\nu)(u, w), \tag{3.8), (3.9}$$

$$\bar{v} = r_0 v/K_c, \tag{3.10}$$

$$\bar{\psi} = \psi/2\nu r_0. \tag{3.11}$$

Then from (1.4),

$$\eta = \bar{r}^2/\bar{t}. \tag{3.12}$$

4. Description and discussion of three-cell vortices

Detailed description of the numerically calculated one- and two-cell solutions will not be given since such solutions are qualitatively similar to the one- and two-cell analytical solutions described in I. The present numerical work does, however, reveal a new family of solutions which are not typified by any known analytical solution. These are the three-cell solutions obtained when $0 > \gamma > -1$ and $2\gamma - 2 < A < A_1(\gamma)$ (see figure 1).

A typical three-cell solution of this family, obtained when $\gamma = -0{\cdot}6$ and $A = -2{\cdot}5$, will now be considered in some detail. (For this value of γ, $A_1 = -2{\cdot}37$, see figure 1.) The computed values of f', f and h for these values of γ and A are plotted in figures 6–8 respectively.

The behaviour of the radial velocity is deduced from the appropriate curve ($A = -2{\cdot}5$) in figure 7 which gives $f(= -\bar{r}\bar{u})$ plotted as a function of η. There are two non-zero values of η called η_2 and η_4 for which f, and therefore the radial velocity, is zero. Thus the flow consists of three cells separated by the time-dependent cylindrical surfaces $\eta = \eta_2$ and $\eta = \eta_4$. When $\eta_2 < \eta < \eta_4$ then $f > 0$ and so there is radial inflow in the middle cell. When $\eta < \eta_2$ and $\eta > \eta_4$ then $f < 0$ and there is radial outflow in the inner and outer cells.

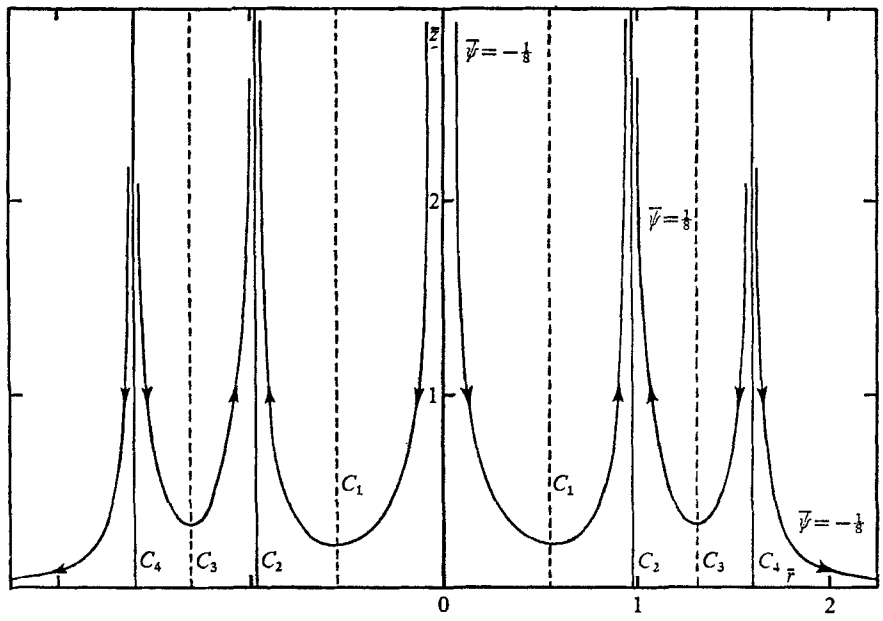

FIGURE 9. The stream surfaces when $\gamma = -0{\cdot}6$, $A = -2{\cdot}5$ and $\bar{t} = 0{\cdot}5$.

Similarly, the behaviour of the axial velocity is deduced from the appropriate curve in figure 6, which gives $f'(= \bar{t}\bar{w}/2\bar{z})$ plotted as a function of η. There are two values of η – for which f', and therefore the axial velocity, is zero – called η_1 and η_3, where $\eta_1 < \eta_2 < \eta_3 < \eta_4$. The axial velocity is upwards when $\eta_1 < \eta < \eta_3$ and downwards outside this range. For the particular case under consideration, $\eta_1 = 0{\cdot}4$, $\eta_2 = 1{\cdot}9$, $\eta_3 = 3{\cdot}4$ and $\eta_4 = 5{\cdot}2$.

These features of the three-cell vortex are illustrated in figure 9 in which certain streamlines are plotted at a particular instant, $\bar{t} = 0{\cdot}5$. The radii corresponding to $\eta = \eta_1$, η_2, η_3 and η_4 are labelled in figure 9 by C_1, C_2, C_3 and C_4 respectively. As time increases the surfaces C_i ($i = 1, 2, 3, 4$) expand radially.

The timewise development of the radial, $\bar{u}$, and axial, $\bar{w}$, velocity components is shown in figures 10 and 11 respectively. Each velocity component is plotted as a function of $\bar{r}$ at three different times, $\bar{t} = 0{\cdot}5$, 1 and 1·5. The corresponding asymptotic values of $\bar{u}$ and $\bar{w}$, specified by the outer potential flow solution given

in (1.8) and (1.10), are also plotted. The behaviour of $\bar{u}$ and $\bar{w}$ at any instant is as described above. Figures 10 and 11 show that the maximum radial and axial velocities in the inner cells decrease as time increases.

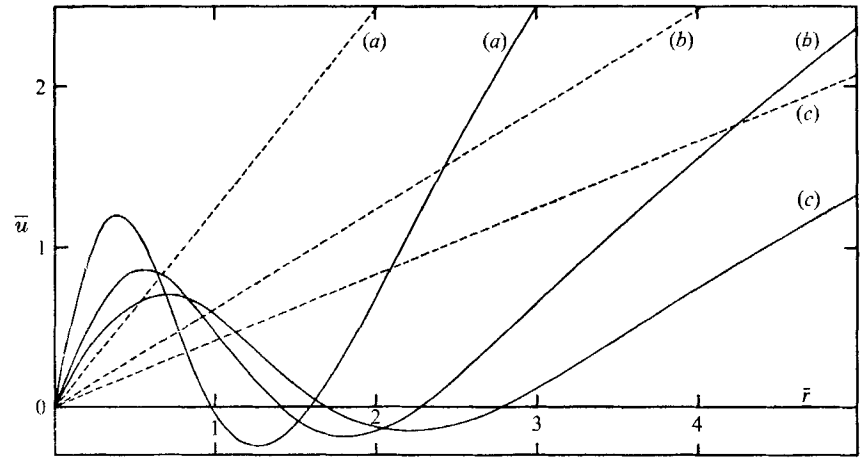

FIGURE 10. The radial velocity distribution for the three-cell solution obtained when $\gamma = -0{\cdot}6$ and $A = -2{\cdot}5$ (solid lines) and the corresponding asymptotic solution (broken lines): $\bar{t} = 0{\cdot}5$, 1 and 1·5, respectively, for curves (*a*), (*b*) and (*c*).

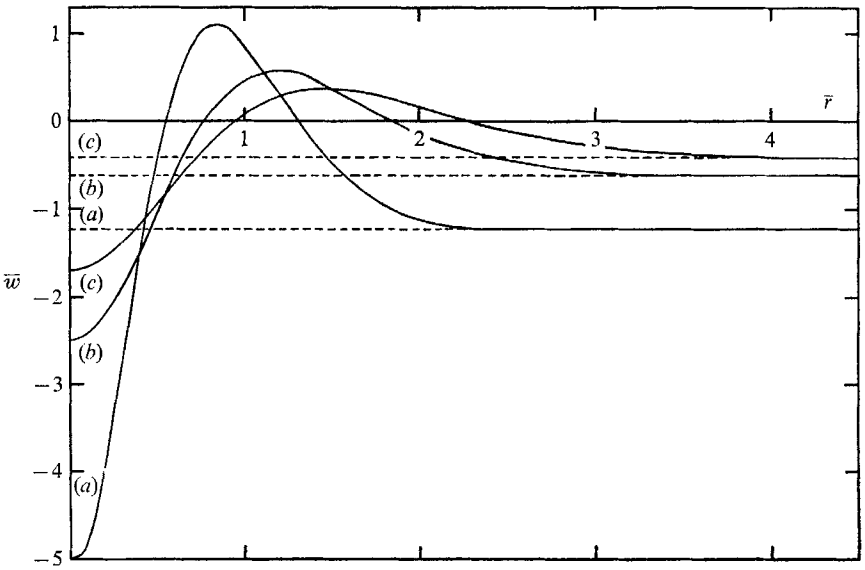

FIGURE 11. The axial velocity distribution for the three-cell solution obtained when $\gamma = -0{\cdot}6$ and $A = -2{\cdot}5$ (solid lines) and the corresponding asymptotic solution (broken lines): $\bar{t} = 0{\cdot}5$, 1 and 1·5, respectively, for curves (*a*), (*b*) and (*c*).

Now, for viscous vortex cores the vorticity tends to diffuse radially outwards. This diffusion process can be balanced only when there is sufficient convection of fresh circulation from outside the vortex core due to radial inflow, as in the case of the steady one- and two-cell vortices (Sullivan 1959). For the present

three-cell vortices, however, there is always radial outflow in the outer cell which results in the convection outwards of circulation which is lower than the circulation of the ambient potential flow. Thus the diffusion and convection processes result in the timewise expansion of the cells and reduction of the maximum radial and axial velocities in the two inner cells.

In figure 12 the circumferential velocity is plotted at $\bar{t} = 0{\cdot}5$, 1 and 1·5. Vertical strokes indicate the radial stations at which the axial velocity is zero. The velocity profiles are similar to those obtained from the analytical solutions and will not be discussed further.

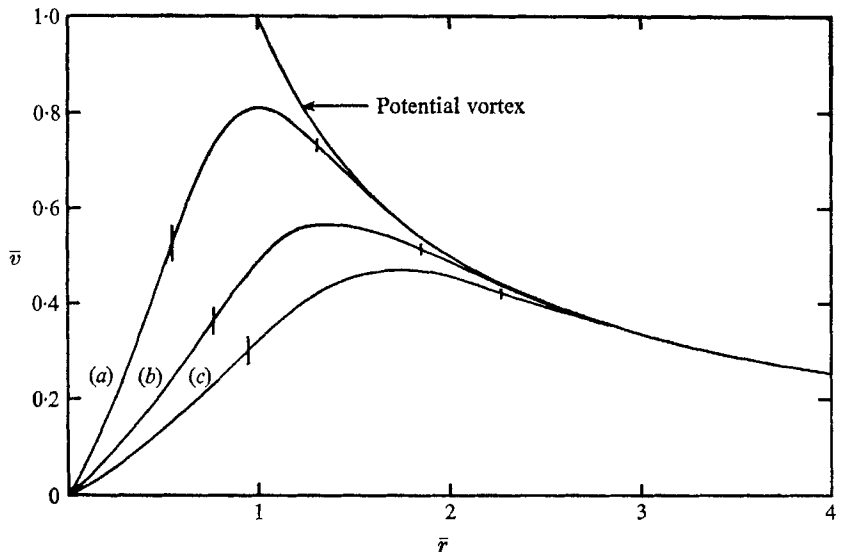

FIGURE 12. The circumferential velocity distribution for the three-cell solution obtained when $\gamma = -0{\cdot}6$ and $A = -2{\cdot}5$, $\bar{t} = 0{\cdot}5$, 1 and 1·5, respectively, for curves (*a*), (*b*) and (*c*).

It has been seen that the numerical method reveals a family of three-cell solutions. Now, another interesting feature of the present work will be discussed. The numerical method provides a continuous range of solutions between any three-cell solution and the analytical one-cell solution. For example, when $\gamma = -0{\cdot}6$ the analytical one-cell solution is given by $A = -0{\cdot}6$ and a typical three-cell solution by $A = -2{\cdot}5$. Now there are solutions for all intermediate values of A and so the gradual development of the three-cell vortex from the one-cell vortex can be traced by considering how the solutions develop as A decreases from $-0{\cdot}6$ to $-2{\cdot}5$. The streamlines for a few intermediate values of A, namely $A = -1{\cdot}86$, $-2{\cdot}20$ and $-2{\cdot}37$ ($= A_1$) are shown in figure 13 by curves (*a*), (*b*) and (*c*), respectively.

Initially, when $A = -0{\cdot}6$, the streamlines are concave upwards since everywhere the axial velocity is downwards and radial velocity outwards. When $A = -1{\cdot}86$ the streamlines have developed a point of inflexion at which the axial velocity is zero, see figure 13, curve (*a*). As A decreases further the point of inflexion develops to give a maximum and minimum. This results in an annular

region of axial upflow, see figure 13, curve (*b*). As $A \to -2{\cdot}37$, the axial position of the maximum tends to infinity. In the limiting case, $A = -2{\cdot}37$ $(= A_1)$, there is a cylinder on which both the axial and radial velocities are zero, see figure 13, curve (*c*). As A decreases further a new cell appears in the region of this cylinder to give a three-cell configuration as in figure 9.

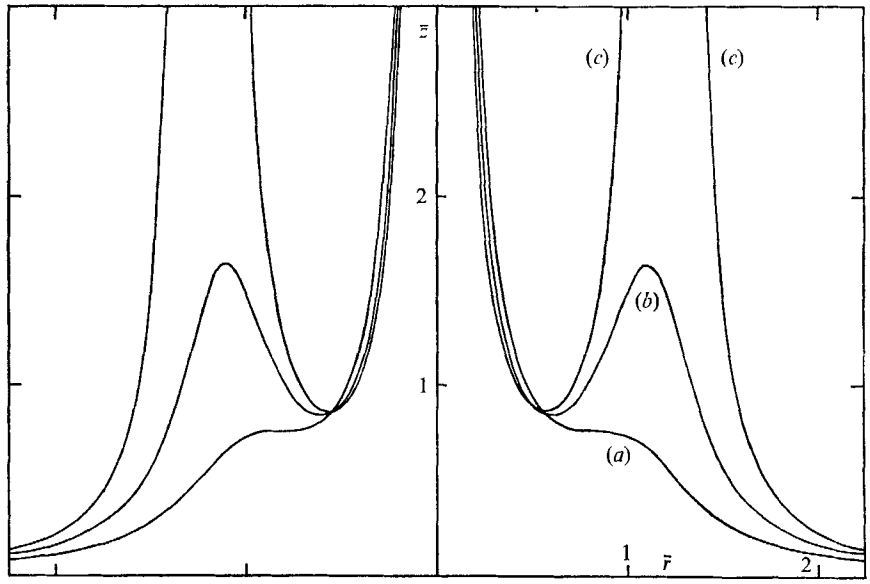

FIGURE 13. The stream surfaces when $\gamma = -0{\cdot}6$, $\bar{t} = 0{\cdot}5$ and $\bar{\psi} = -0{\cdot}5$: $A = -1{\cdot}86$, $-2{\cdot}2$ and $-2{\cdot}37$, respectively, for curves (*a*), (*b*) and (*c*).

A possible physical explanation of the early stages of the transition may be that the radial outflow is insufficient to drain the increasing volume of fluid carried towards the plane $z = 0$ due to the increasing axial downflow near the axis of symmetry. Hence there is a tendency for fluid to be emitted axially as well as radially.

Gutman (1957) showed that when thermal effects are taken into account the inner cell of a two-cell vortex corresponds to a closed cell of recirculating fluid around the axis bounded above by a free stagnation point on the axis. Similarly, the middle cell of a three-cell vortex may correspond to an axially bounded torroidal region of recirculating fluid over which fluid flows radially outwards from the inner to the outer cell.

5. Conclusions

The present numerical work extends the results of the analytical work of I in several respects. First, a new family of solutions is discovered namely the three-cell vortices, which are not represented by any known analytical solution. These solutions are obtained when there is a suitable radial outflow in the ambient potential flow and when the axial velocity on the axis lies within a certain range of negative values.

Second, the numerical solutions suggest how a three-cell (or two-cell) solution can gradually develop from a one-cell solution. The analytical solutions failed to do this because they represented particular solutions for two discrete values of A and provided no solutions for intermediate values of A.

Third, the present work shows the sensitivity of the core flow to small changes in the outer flow. When many solutions are possible for a fixed value of γ each solution is characterized by a value of A which also corresponds to a specific value of B in (1.11). For example, when $A = \gamma$ equation (1.24) shows that $B = 0$ and when $A = -2\gamma$ (1.26) shows that $B = -3\gamma/(1+\gamma)$. (For other values of A the corresponding values of B can be measured from graphs such as in figure 7.) To the first order however, the outer potential flow is specified solely by γ and is independent of B whereas the core flow is characterized by A which represents the axial velocity on the axis.

For steady flows Donaldson & Sullivan (1960, 1963) showed, using numerical techniques similar to those used in the present work, that no asymptotic solutions exist other than the one and two-cell analytical solutions of Burgers (1940, 1948) and Sullivan (1959), respectively. Thus steady flow solutions are similar to the category of unsteady solutions, obtained when $\gamma > \frac{1}{2}$, which were discussed in § 3. For flows of this type there are no three-cell solutions and there can apparently be no gradual transition from a one-cell to a two-cell solution.

The author is indebted to Professor N. H. Johannesen in whose department this work was done and to Dr I. M. Hall under whose guidance this paper was produced. During the course of this work the author held a Research Studentship from the Science Research Council.

Appendix. The perturbed analytical one-cell solution

The numerical results showed that when $-1 < \gamma < \frac{1}{2}$ solutions other than the analytical one- and two-cell solutions were possible. It was noted in § 2 that the analytical one-cell solution satisfies the outer boundary conditions only if $\gamma > -1$. In this appendix it is assumed that if solutions in addition to the analytical solutions exist (for a fixed value of γ) they will include solutions corresponding to a slightly perturbed analytical one-cell solution. Then, using the inequality $\gamma > -1$, it is shown that this perturbed solution cannot satisfy the outer boundary conditions if $\gamma > \frac{1}{2}$.

Thus a solution of (1.14) of the form

$$f(\eta) = \gamma\eta + \delta G(\eta) \tag{A 1}$$

is considered, where δ is small and G is a function of η. Boundary condition (1.7) gives

$$G(0) = 0.$$

Substituting (A 1) into (1.14) and neglecting powers of δ greater than one gives

$$[\eta G'' + \eta G']' + \gamma\eta G'' - 2\gamma G' = 0. \tag{A 2}$$

On putting $x = -(1+\gamma)\eta$

and $\phi(x) = G'(\eta)$,

(A 2) reduces to the confluent hypergeometric equation

$$x\frac{d^2\phi}{dx^2}+(1-x)\frac{d\phi}{dx}-\left(\frac{1-2\gamma}{1+\gamma}\right)\phi=0.$$

The solution of this equation which satisfies the boundary conditions on the axis is

$$\phi = C\,{}_1F_1\left(\frac{1-2\gamma}{1+\gamma};1;x\right),$$

where C is a constant and ${}_1F_1$ is the confluent hypergeometric function. Now when η is large, x is large and negative since $1+\gamma>0$, but for x real, large and negative (Morse & Feshbach 1953),

$${}_1F_1(a;d;x)\sim\frac{\Gamma(d)}{\Gamma(d-a)}(-x)^{-a},$$

where a and d are constants and Γ is the gamma function. Hence for large values of η, corresponding to large negative values of x,

$$\phi\to\frac{C}{\Gamma(3\gamma/1+\gamma)}(-x)^{(2\gamma-1)/(\gamma+1)}.$$

Now $(-x)^{(2\gamma-1)/(\gamma+1)}$ tends to zero or infinity according as $\gamma<\frac{1}{2}$ or $\gamma>\frac{1}{2}$. Thus if $\gamma>\frac{1}{2}$ the perturbed analytical one-cell solution cannot satisfy the outer boundary conditions.

REFERENCES

Bellamy-Knights, P. G. 1970 An unsteady two-cell vortex solution of the Navier–Stokes equations. *J. Fluid Mech.* **41**, 673.

Burgers, J. M. 1940 Application of a model system to illustrate some points of the statistical theory of free turbulence. *Proc. Acad. Sci. Amst.* **43**, 2–12.

Burgers, J. M. 1948 A mathematical model illustrating the theory of turbulence. *Adv. Appl. Mech.* **1**, 197–199.

Donaldson, C. du P. & Sullivan, R. D. 1960 Examination of the solutions of the Navier–Stokes equations for a class of three-dimensional vortices. Part I. Velocity distributions for steady motion. *Aero. Res. Assoc. Princeton Rep.* (AFOSR TN 60-1227).

Donaldson, C. du P. & Sullivan, R. D. 1963 Examination of the solutions of the Navier–Stokes equations for a class of three-dimensional vortices. Part III. Temperature distributions for steady motion. *Aero. Res. Assoc. Princeton Rep.* no. 51 (AFOSR TN 60-1227).

Gutman, L. N. 1957 Theoretical model of a waterspout. *Bull. Acad. Sci. U.S.S.R. (Geophysics series)* **1**, 79.

Morse, P. M. & Feshbach, H. 1953 *Methods of Theoretical Physics.* McGraw-Hill.

Morton, B. R. 1966 Geophysical vortices. *Progress in Aeronautical Sciences*, **7**, 145–194.

Rott, N. 1958 On the viscous core of a line vortex. *Z. angew. Math. Phys.* **9***b*, 543–553.

Rott, N. 1959 On the viscous core of a line vortex. II. *Z. angew. Math. Phys.* **10**, 73–81.

Sullivan, R. D. 1959 A two-cell solution of the Navier–Stokes equations. *J. Aerospace Sci.* **26**, 767.